

Santa Clara University

Scholar Commons

Physics

College of Arts & Sciences

2-2021

Photoelectric absorption cross section of silicon near the bandgap from room temperature to sub-Kelvin temperature

C. Stanford

M. J. Wilson

B. Cabrera

M. Diamond

N. A. Kurinsky

See next page for additional authors

Follow this and additional works at: <https://scholarcommons.scu.edu/physics>



Part of the [Physics Commons](#)

Recommended Citation

"Photoelectric Absorption Cross Section of Silicon Near the Bandgap from Room Temperature to Sub-Kelvin Temperature", C. Stanford, M.J. Wilson, B. Cabrera, M. Diamond, N. A. Kurinsky, R. A. Moffatt, F. Ponce, B. von Krosigk, B. A. Young, AIP Advances 11, 025120 (2021).

© 2021 Author(s). All article content, except where otherwise noted, is licensed under a Creative Commons Attribution (CC BY) license (<http://creativecommons.org/licenses/by/4.0/>).






This Article is brought to you for free and open access by the College of Arts & Sciences at Scholar Commons. It has been accepted for inclusion in Physics by an authorized administrator of Scholar Commons. For more information, please contact rscroggin@scu.edu.

Authors

C. Stanford, M. J. Wilson, B. Cabrera, M. Diamond, N. A. Kurinsky, R. A. Moffatt, F. Ponce, B. von Krosigk, and Betty A. Young

RESEARCH ARTICLE | FEBRUARY 10 2021

Photoelectric absorption cross section of silicon near the bandgap from room temperature to sub-Kelvin temperature

C. Stanford ; M. J. Wilson ; B. Cabrera ; M. Diamond; N. A. Kurinsky; R. A. Moffatt; F. Ponce ; B. von Krosigk ; B. A. Young



AIP Advances 11, 025120 (2021)

<https://doi.org/10.1063/5.0038392>

 CHORUS



Articles You May Be Interested In

Study of high- and low-work-function surfaces for hyperthermal surface ionization using an absolute Kelvin probe

J. Vac. Sci. Technol. A (July 2001)

What was measured in Millikan's study of the photoelectric effect?

Am. J. Phys. (September 2015)

Graphene-insulator-semiconductor capacitors as superior test structures for photoelectric determination of semiconductor devices band diagrams

AIP Advances (May 2018)



Special Topics Open for Submissions

[Learn More](#)

Photoelectric absorption cross section of silicon near the bandgap from room temperature to sub-Kelvin temperature

Cite as: AIP Advances 11, 025120 (2021); doi: 10.1063/5.0038392

Submitted: 24 November 2020 • Accepted: 3 January 2021 •

Published Online: 10 February 2021



View Online



Export Citation



CrossMark

C. Stanford,^{1,2,a)} M. J. Wilson,^{3,4} B. Cabrera,^{1,5,b)} M. Diamond,³ N. A. Kurinsky,^{6,7} R. A. Moffatt,¹ F. Ponce,¹ B. von Krosigk,⁴ and B. A. Young⁸

AFFILIATIONS

¹Department of Physics, Stanford University, Stanford, California 94305, USA

²Department of Physics, Harvard University, Cambridge, Massachusetts 02138, USA

³Department of Physics, University of Toronto, Toronto, Ontario M5S 1A7, Canada

⁴Institut für Experimentalphysik, Universität Hamburg, 22761 Hamburg, Germany

⁵SLAC National Accelerator Laboratory/Kavli Institute for Particle Astrophysics and Cosmology, 2575 Sand Hill Road, Menlo Park, California 94025, USA

⁶Fermi National Accelerator Laboratory, Center for Particle Astrophysics, Batavia, Illinois 60510, USA

⁷Kavli Institute for Cosmological Physics, University of Chicago, Chicago, Illinois 60637, USA

⁸Department of Physics, Santa Clara University, Santa Clara, California 95053, USA

^{a)} Author to whom correspondence should be addressed: cstanford@g.harvard.edu

^{b)} Electronic mail: cabrera@stanford.edu

ABSTRACT

The use of cryogenic silicon as a detector medium for dark matter searches is gaining popularity. Many of these searches are highly dependent on the value of the photoelectric absorption cross section of silicon at low temperatures, particularly near the silicon bandgap energy, where the searches are most sensitive to low mass dark matter candidates. While such cross section data have been lacking from the literature, previous dark matter search experiments have attempted to estimate this parameter by extrapolating it from higher temperature data. However, discrepancies in the high temperature data have led to order-of-magnitude differences in the extrapolations. In this paper, we resolve these discrepancies by using a novel technique to make a direct, low temperature measurement of the photoelectric absorption cross section of silicon at energies near the bandgap (1.2 eV–2.8 eV).

© 2021 Author(s). All article content, except where otherwise noted, is licensed under a Creative Commons Attribution (CC BY) license (<http://creativecommons.org/licenses/by/4.0/>). <https://doi.org/10.1063/5.0038392>

The photoelectric absorption cross section ($\sigma_{\text{p.e.}}$) of silicon at low temperatures is an important parameter for modern experiments that use cryogenic silicon as a substrate for the direct detection of dark matter.^{1–5} Several dark matter signal models depend on this parameter. We have discussed these models in more detail in Ref. 6, but we will highlight two of them here.

First, the hypothesized kinetic mixing of dark photons and Standard Model photons results in an expected interaction between dark photons and electrons with a cross section given by⁷

$$\sigma_{A'}(E_{A'}) = \frac{\epsilon^2}{\beta_{A'}} \sigma_{\text{p.e.}}(E_{A'}), \quad (1)$$

where $E_{A'}$ is the dark photon's total energy, $\beta_{A'} = v_{A'}/c$ is the dark photon's relativistic beta factor, and ϵ is the kinetic mixing parameter.

Second, the expected cross section for the interaction of axion-like particles (ALPs) with electrons is given by^{8,9}

$$\sigma_a(E_a) = \sigma_{\text{p.e.}}(E_a) \frac{g_{ae}^2}{\beta_a} \frac{3E_a^2}{16\pi\alpha m_c^2 c^4} \left(1 - \frac{\beta_a^{2/3}}{3}\right), \quad (2)$$

where E_a is the ALP's total energy, $\beta_a = v_a/c$ is its relativistic beta factor, α is the fine structure constant, m_e is the mass of the electron, and g_{ae} is the axioelectric coupling of the ALP to the electrons.

Note that in both (1) and (2), the interaction rate is directly dependent on the value of $\sigma_{p.e.}$. We performed an exhaustive literature search^{10–18} for measurements of $\sigma_{p.e.}$ at low energies (< 10 eV), where silicon dark matter experiments are most competitive, but we found the data to be lacking for the temperature regime of interest (< 5 K). Although previous dark matter search experiments have attempted to account for the temperature dependence of $\sigma_{p.e.}$ by extrapolating from the data found in the aforementioned literature search,^{1,2} discrepancies in the high temperature data have led to low temperature projections that differ by more than an order of magnitude at energies near the silicon bandgap. The result is a dominating uncertainty in any experimental sensitivity curve for dark matter models that depend on $\sigma_{p.e.}$. This limitation was the motivation for the direct measurement of $\sigma_{p.e.}$ at sub-Kelvin temperatures.

To measure $\sigma_{p.e.}$, we designed an experiment in which a monochromatic light beam was sent through several silicon “filters” with varying thicknesses. Then, by comparing the relative transmission, a value for $\sigma_{p.e.}$ was obtained, free from many of the systematics that would be present in an absolute transmission measurement.

The experiment was performed in the same ^3He cryostat used to previously measure charge propagation in silicon and germanium at low temperatures.^{19–22} The cryostat was retrofitted with a new 50/125 multi-mode fiber optic (FO) via a vacuum feedthrough. The FO was used to illuminate samples at the cold stage with various external light sources (LED/laser diode) of differing wavelengths (see Table I). At the base-temperature stage, the FO was directly coupled to a lens. The beam was focused to a diameter of ~ 200 μm onto a filter mount roughly 150 mm away via a 2-axis MEMS mirror, as illustrated in Fig. 1. The MEMS mirror tilt controls the x - y position of the incident beam on the filter mount, with the relaxed state set to the center of the filter mount. Thus, the angle of incidence to any radially symmetric point on the filter mount was the same.

The filter mount was made from a 6 cm^2 brass plate, illustrated in Fig. 2. The front side had eight 0.5 mm diameter through-holes radially symmetric to the mount center. Adjacent holes were 2 mm apart, center-to-center. The back side had 1.6×1.6 mm^2 indents, each centered on a through-hole and used to mount a 1.5×1.5 mm^2 piece of silicon that was held in place with GE varnish. The silicon

TABLE I. In order to measure the photoelectric absorption cross section over a range of energies, a series of diodes with known wavelengths was used. The transmission curves provided by the manufacturer are summarized in the peak, lower half-maximum (LHM), and upper half-maximum (UHM) columns. They were controlled with a Thorlabs DC2200 LED Driver.

Peak (nm)	LHM (nm)	UHM (nm)	Peak (eV)	Type
450	447	449	2.77	Laser
530	521	547	2.34	LED
639.5	639	640	1.94	Laser
660	651	667	1.88	LED
787	786	788	1.58	Laser
950	905	970	1.31	LED
972	970	973	1.28	Laser
1028	1027	1029	1.21	Laser

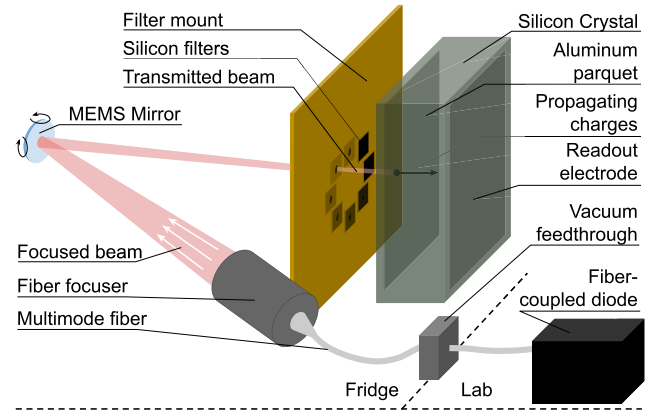


FIG. 1. The detector, which consisted of a 1 cm \times 1 cm \times 4 mm crystal of high-purity silicon, and the laser mechanism, which used a MEMS mirror to scan a focused beam of light pulses across the back face of the crystal in order to produce a 2D image. The crystal was biased via a parquet electrode on the illuminated face.

samples used in this work were cut from seven thinned, boron-doped ($\rho < 100$ $\Omega\text{-cm}$) CZ Prime (100) wafers with thicknesses in micrometers of 5.1 ± 0.1 , 10.0 ± 0.1 , 24.0 ± 0.2 , 49.4 ± 0.1 , 100.2 ± 0.1 , 149.7 ± 0.2 , and 198.8 ± 0.1 . One indent remained empty for calibration purposes.

Approximately 3 mm behind the filter mount (relative to the oncoming photon beam) was a silicon crystal that acted as the detector. This crystal was cut from a 4 mm-thick wafer of undoped ultra-high-purity float-zone silicon (~ 15 $\text{k}\Omega\text{-cm}$). The residual impurity was measured to be p-type with a concentration of 10^{12} cm^{-3} . The front (facing the oncoming beam) and back faces of the crystal were 1 cm \times 1 cm. The front face was patterned with an aluminum–tungsten mesh electrode, with 20% coverage,²³ which was used to bias the crystal to 50 V cm^{-1} . The back face was covered almost fully with an aluminum thin film that served as a ground electrode.

The silicon filters were individually illuminated with photons of different wavelengths by manipulating the MEMS mirror. The transmission through the silicon filters was measured as a charge signal in the silicon crystal detector. The charge was collected externally through an amplifier circuit by using the data acquisition system (DAQ).

The data-taking procedure was as follows. First, the fridge was set to the desired temperature, and a light source was connected to the fiber leading into the fridge. The options for light sources spanned a range of wavelengths, summarized in Table I. Then, a run was performed at that temperature and wavelength. A run involved a scan of the beam spot over each hole, with each scan involving a 14×14 grid of individual measurements. To make a single measurement, the diode was pulsed in a train of 32 pulses using a Thorlabs DC2200 LED Driver. The pulses had widths of 20 μs (some diodes required longer widths), spaced 8 ms apart. These pulses traveled down the fiber, out the focuser, and bounced off the MEMS mirror, which directed them through one of the holes in the filter mount. Then, some of the light from each pulse reflected off the silicon filter present in that hole, while another fraction of the light was absorbed

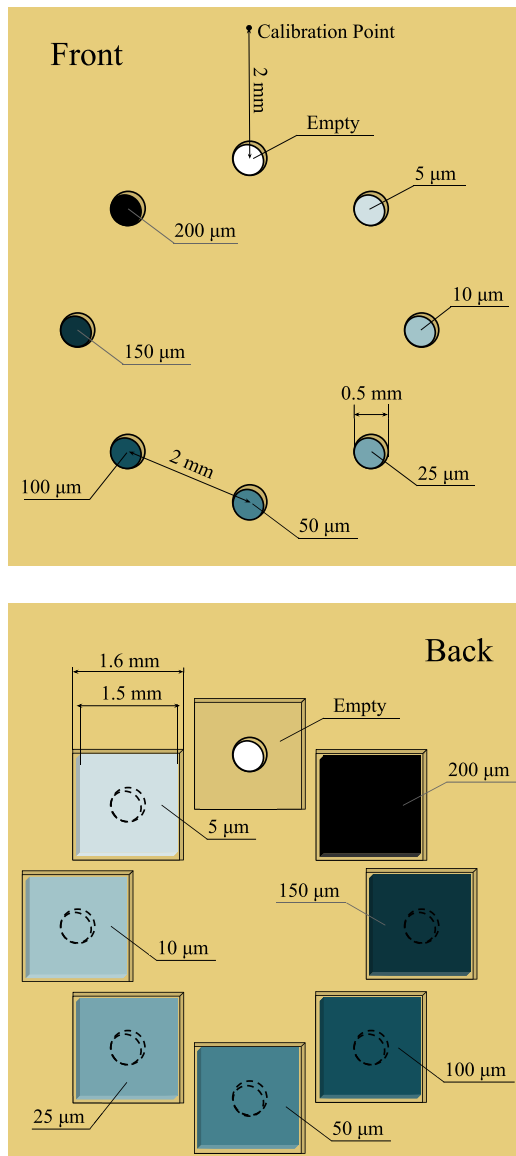


FIG. 2. Top: the front (facing the beam) of the filter mount featured 8 holes arrayed in a circular pattern. When the mirror was at rest, the beam spot fell in the center of the circle. This was done so that the angle of incidence of the beam at each hole (and therefore the amount of reflected light) was the same. At a distance of 2 mm radially outward from the empty hole, a calibration point was designated to measure spillover light from the beam spot into neighboring holes. Bottom: the back (facing the detector crystal) of the filter mount featured square indents aligned with each hole, which held pieces of silicon with different thicknesses. Each piece of silicon was held in place using two small spots of GE varnish at opposing corners.

by the filter. The remaining fraction was transmitted through the filter and detected.

To ensure proper alignment between the beam spot and the center of each hole, first a rough x-y value for each hole center was estimated, and then, a 14×14 grid of x-y positions was made for each hole, covering a $0.6 \text{ mm} \times 0.6 \text{ mm}$ area surrounding that hole's estimated center. Measurements were then taken at each point in

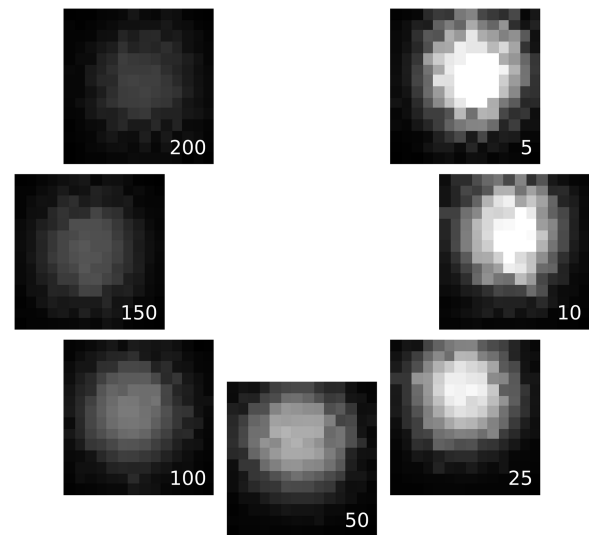


FIG. 3. A run using the 950 nm diode at 0.5 K. The run involved a scan over each hole containing a silicon filter. Each scan involved a set of 14×14 measurements so that the values corresponding to a precise alignment of the beam spot and the hole could be used for the analysis. The white text indicates the thickness of the silicon filter (in μm) corresponding to each scan.

these grids in order that the maximum values for the charge collection, corresponding to precise alignment of the beam spot with a hole, could be used for the analysis.

Furthermore, to eliminate any temporal effects from biasing the results (such as a small increase in fridge temperature over the course of the run), rather than performing the scan over each hole one after another in sequence, the x-y points from all the separate scans were combined and shuffled so that the order of measurements favored no hole in particular.

To reduce the effect of charge buildup in the crystal over time, the crystal was grounded between every measurement. While grounded, the mirror was used to direct the beam spot toward the open hole, and a 1 ms flash of light was sent into the crystal to aid in the neutralization of the charge buildup. Then, the voltage was reapplied to the crystal so that the next measurement could be taken.

Since each measurement involved a train of 32 light pulses, each voltage trace recorded by using the DAQ was split into 32 sections and summed together to form an average pulse. The amplitude of the average pulse was used as a measure of the total amount of light transmitted through the silicon and collected by the crystal during that measurement.

In order to compare two different pulse amplitudes, an absolute calibration of the detector response was needed. This was done in two steps. First, a diode was connected to the system, and the mirror directed the beam spot toward the open hole. Then, a sweep over applied current to the diode was performed, and the average pulse size at each value of the applied current was observed and recorded. Second, the same diode was placed in a dark box with a photomultiplier tube capable of counting single photoelectrons. Using the same sweep over applied current as before, an absolute measure of the crystal response to a given amount of light was obtained. What was found was that the crystal responds linearly with

incident light up until average voltage pulses of 2 V, after which it begins to saturate. In the majority of runs, the width of the laser pulses was tuned so that the pulse sizes remained within this linear range, but in some cases, the average pulse amplitude extended outside this range, and the absolute calibration was used to correct that amplitude.

The average amplitudes from all the measurements in each scan were then used to produce a 2D image of that scan to visually confirm that the scan was in fact aligned with a hole. The set of scan images for one of the runs can be seen in Fig. 3, where a decrease in amplitude is seen as the thickness of silicon increases.

To turn a set of scans into a value for the photoelectric absorption cross section, a series of post-processing steps was performed.

First, the set of 14×14 points for each scan was divided into thirds based on the time of acquisition, representing the first third of points taken for that scan, the second third, and the final third. Since the points for all the scans were taken in a random order, this process effectively separated each scan into 3 “sub-scans” of lower resolution.

Second, in order to reduce the impact of outliers, the median of the top 5 amplitudes for each sub-scan was taken as the transmission value for that sub-scan. Finally, these three sub-scan transmission values were taken together, and the median of those values was taken as the transmission value for the whole scan. This reduced the impact of any transient effects at the start of a run that were present in only the first sub-scan.

Once these transmission values were obtained, they were plotted against the corresponding silicon thickness. The results from several runs taken at 0.5 K are shown in Fig. 4 (top). Note that some runs include more points than others. This is because the shorter wavelength light used for some of the runs could not be detected through the thicker pieces of silicon.

The error bars for these points were the result of a detailed study, which checked for biases introduced by various effects, such as bias voltage, light intensity, linearity correction, neutralization procedure, and day-to-day variability. However, due to the symmetric nature of the data-taking process, these were all found to be sub-dominant to the primary source of error, which was caused by the filter mount itself. This was determined by performing a calibration run where each hole of the filter mount was left empty. The standard deviation in the light collection through the eight holes in this case was measured to be $\sim 3\%$, with a small dependence on the wavelength. A run with another mount produced by the same machining process resulted in a different variation from hole to hole but with the same overall magnitude of variation. Since this was the dominant source of error, the standard deviation of light collection found in this calibration run was used to set the error bars in Fig. 4 (top).

After plotting, the points were fit with an exponential according to the Beer–Lambert law,

$$Ae^{-\rho\sigma_{p.e.}x}, \quad (3)$$

where A (arbitrary constant) and $\sigma_{p.e.}$ are fit parameters, ρ is the density of silicon (2.33 g cm^{-3}), and x is the silicon thickness.

These fitted values for $\sigma_{p.e.}$ at 0.5 K are shown in Fig. 4 (bottom). Each fitted value is presented as an ellipse, with the height

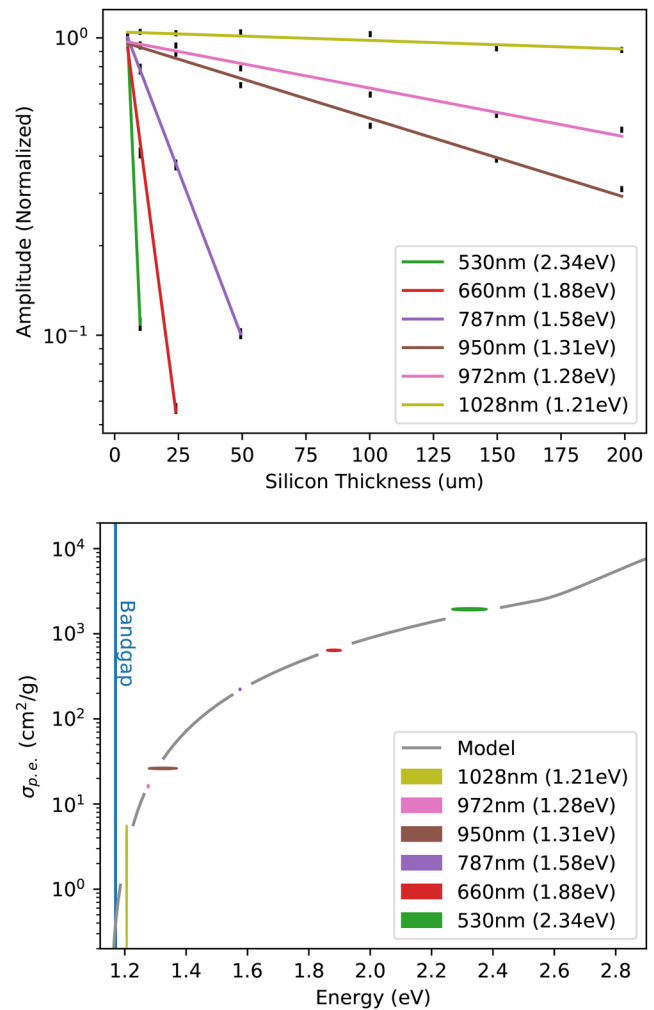


FIG. 4. Top: the normalized transmission through the different thicknesses of silicon for multiple wavelengths of light at 0.5 K. The error bars are dominated by systematic errors introduced by the filter mount. The negative of each fitted slope gives the value of the photoelectric absorption cross section at the corresponding wavelength. Bottom: the values of $\sigma_{p.e.}$ at 0.5 K from above, plotted in energy space. Each fitted value is presented as an ellipse, with the height representing the uncertainty of the fit and the width representing the uncertainty in the diode wavelength.

representing the statistical uncertainty in the fit and the width representing the uncertainty of the diode energy. For the energy uncertainty, the lower and upper bounds were calculated from the upper half-maximum wavelength and lower half-maximum wavelength of the emission spectrum, respectively (see Table I).

The photoelectric absorption cross section is not expected to differ significantly between 0 K and the 0.5 K results presented in this paper. However, it does increase at warmer temperatures. We confirmed this effect by repeating the 0.5 K measurements at 5 K, 77 K, and 295 K. We also performed some continuous measurements at a fixed wavelength as the fridge was warming up. These data are summarized in Fig. 5. We did not measure a

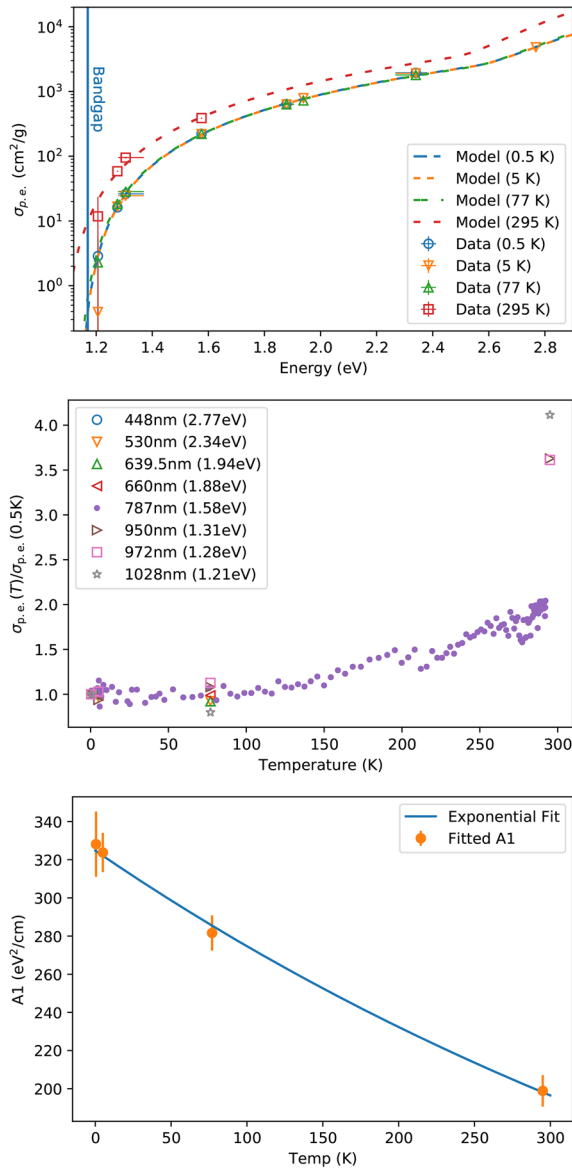


FIG. 5. Top: measurements of $\sigma_{p.e.}$ at four discrete temperatures and the results of a simultaneous fit across all four temperatures using the model described in the text. Middle: the temperature dependence of $\sigma_{p.e.}$ relative to $T = 0.5$ K. The cross section for 787 nm was measured continuously as the fridge warmed up, while the cross sections for the other wavelengths were only measured at four discrete temperatures. We did not measure a statistically significant difference in the cross section for temperatures of 77 K and below. Bottom: when the model includes an independent parameter for the first indirect bandgap proportionality constant (A_1) at each of the four measured temperatures, the fitted values follow an exponential curve.

statistically significant difference in $\sigma_{p.e.}$ for temperatures up to 77 K but did observe an upward trend in $\sigma_{p.e.}$ between 77 K and 295 K.

To set a dark matter limit, a continuous curve in $\sigma_{p.e.}$ -energy space is preferred. To obtain this curve, we fit the discrete

measurements to a model describing the temperature-dependent absorption coefficient $\alpha(T)$ via direct and indirect photon absorption,²⁴

$$\alpha(T) = \sigma_{p.e.}(T)\rho_{Si} = \sum_{i,j=1,2} C_i A_j \left[\frac{(E_\gamma - E_{gj}(T) + E_{pi})^2}{e^{E_{pi}/kT} - 1} + \frac{(E_\gamma - E_{gj}(T) - E_{pi})^2}{1 - e^{-E_{pi}/kT}} \right] + A_d (E_\gamma - E_{gd}(T))^{1/2}, \quad (4)$$

where E_γ is the photon energy, k is the Boltzmann constant, the first and second terms in the sum describe indirect photon absorption via phonon absorption and emission, respectively, and the last term describes direct photon absorption. The suffix i refers to the two phonon energies from the transverse acoustic (TA) ($E_p = 18.27$ meV) and transverse optical (TO) ($E_p = 57.73$ meV) lattice waves considered, and the suffix j refers to the two different indirect bandgaps E_g , which may be active in phonon absorption. We did not explicitly include in the model any direct contributions from possible B_sO_2 complexes^{25,26} in the CZ-grown silicon filters. The C_i coefficients describe the electron-phonon coupling constant; for silicon, $C_{TA} = 5.5$ and $C_{TO} = 4.0$. The A_1 , A_2 , and A_d coefficients are used as proportionality constants.

The temperature-dependent indirect bandgap energies $E_{gj}(T)$ are given by

$$E_{gj}(T) = E_{gj}(0) - \frac{\beta T^2}{T + \gamma}, \quad (5)$$

where $\beta = 7.021 \times 10^{-4}$ eV K⁻¹ and $\gamma = 1108$ K. To improve the fit of the model to the lower energy measurements, we allowed the lowest bandgap energy at 0 K [$E_{g1}(0)$] to float while using the fixed value of $E_{g2}(0) = 2.5$ eV for the second indirect bandgap energy, where there is no enough data to constrain.

The model was fit simultaneously to the four $\sigma_{p.e.}$ measurements taken at 0.5 K, 5 K, 77 K, and 295 K, taking into account the uncertainties in the measured $\sigma_{p.e.}$ values as well as the uncertainties due to the diode wavelength distributions (see Table I). In this fit, $E_{g1}(0)$ was held constant across temperatures, but in order to investigate a possible temperature dependence in A_1 , we allowed A_1 to vary. Only one measurement was taken at an energy above the second indirect bandgap, so the A_2 temperature dependence was not investigated.

The results of the fit for A_2 and $E_{g1}(0)$ are $6(3) \times 10^3$ eV² cm⁻¹ and 1.134(4) eV, respectively. The fit results for A_1 at each of the four temperatures are shown in Fig. 5 (bottom) and demonstrate a significant temperature dependence. This may be a result of temperature-dependent effects that the phenomenological absorption model described in Eq. (4) does not account for, such as the effect of temperature on the density of states and the electron-phonon coupling. In order to improve the model's fit to the $\sigma_{p.e.}$ measurements and produce a result that can be used for dark matter searches, we performed a second iteration of the simultaneous fit, this time constraining A_1 to have an exponential temperature dependence,

$$A_1(T) = c_0 e^{-c_1 T}. \quad (6)$$

Using the previously determined $E_{g1}(0)$ and A_2 as fixed parameters, the fitted c_0 and c_1 values are

$$\begin{aligned} c_0 &= 325(6) \text{ eV}^{-2} \text{ cm}^{-1}, \\ c_1 &= 1.7(1) \times 10^{-3} \text{ K}^{-1}. \end{aligned} \quad (7)$$

The result of this fit is shown in Fig. 5. We chose an exponential function for empirical reasons as it was physically plausible and required few variables to adequately fit the A_1 values.

The result of this second iteration of the simultaneous fit is shown compared to the data in Fig. 4 (bottom) and Fig. 5 (top).

In future work, finer sampling of the photo-electric cross section may be accomplished by modifying the readout to accommodate a filtered xenon flash lamp (TDS) or by modifying the integrator for use with a longer time-constant tunable light source with a conventional shutter, with switching times on the scale of milliseconds. The current work was restricted to pulses from single-wavelength diodes due to the nature of its AC-coupled charge amplifier, designed for fast charge transport measurements rather than integrated power.

Finally, with the active interest in using other (non-silicon) semiconductors in dark matter searches,^{3,27–30} it is worth noting that the technique outlined in this paper can be easily extended to such materials by placing samples of that semiconductor in the filter mount. However, to probe the values of the cross section at photon energies below the silicon bandgap, a detector crystal with a smaller gap, such as germanium, would need to be used.

See the [supplementary material](#) for the data files containing the points and curves in Fig. 5 (top) and for a document describing them.

We would like to thank Yonit Hochberg for initial conversations that led to the design of this experiment, Brian Lenardo for his assistance with the dark box calibration, and Steve Yellin for helpful comments. This work was supported, in part, by the U.S. Department of Energy, the National Science Foundation, the DFG (Germany) under Project No. 420484612, and Germany's Excellence Strategy—EXC 2121 “Quantum Universe”—Grant No. 390833306. The fiber feedthrough and LEDs were provided by the NSERC, Canada. Precision thickness measurements of the silicon filters were provided by Filmetrics (KLA) Application Lab in Santa Clara, CA. This document was prepared by using resources of the Fermi National Accelerator Laboratory (Fermilab), a U.S. Department of Energy, Office of Science, HEP User Facility. Fermilab is managed by Fermi Research Alliance, LLC (FRA), acting under Contract No. DE-AC02-07CH11359. This document was also prepared using resources of SLAC, which is operated under Contract No. DEAC02-76SF00515 by the U.S. Department of Energy.

DATA AVAILABILITY

The data that support the findings of this study are available within its [supplementary material](#).

REFERENCES

- R. Agnese *et al.*, *Phys. Rev. Lett.* **121**, 051301 (2018).
- D. W. Amaral *et al.*, “Constraints on low-mass, relic dark matter candidates from a surface-operated supercdms single-charge sensitive detector,” [arXiv:2005.14067 \[hep-ex\]](#) (2020).
- T. Aralis *et al.* and SuperCDMS Collaboration, *Phys. Rev. D* **101**, 052008 (2020).
- A. Aguilar-Arevalo *et al.* and DAMIC Collaboration, *Phys. Rev. Lett.* **123**, 181802 (2019).
- SENSEI Collaboration, [arXiv:1901.10478 \[hep-ex\]](#) (2019).
- B. von Krosigk *et al.*, “Effect on dark matter exclusion limits from new silicon photoelectric absorption measurements” (submitted).
- I. M. Bloch, R. Essig, K. Tobioka, T. Volansky, and T.-T. Yu, *J. High Energy Phys.* **6**, 87 (2017); [arXiv:1608.02123 \[hep-ph\]](#).
- M. Pospelov, A. Ritz, and M. Voloshin, *Phys. Rev. D* **78**, 115012 (2008); [arXiv:0807.3279 \[hep-ph\]](#).
- C. Fu *et al.* (PandaX), *Phys. Rev. Lett.* **119**, 181806 (2017); [arXiv:1707.07921 \[hep-ex\]](#).
- B. L. Henke, E. M. Gullikson, and J. C. Davis, *At. Data Nucl. Data Tables* **54**, 181 (1993).
- M. A. Green, *Sol. Energy Mater. Sol. Cells* **92**, 1305 (2008).
- M. A. Green and M. J. Keevers, *Prog. Photovoltaics: Res. Appl.* **3**, 189 (1995).
- W. C. Dash and R. Newman, *Phys. Rev.* **99**, 1151 (1955).
- D. F. Edwards, in *Handbook of Optical Constants of Solids*, edited by E. D. Palik (Academic Press, Burlington, 1997), pp. 547–569.
- G. G. Macfarlane, T. P. McLean, J. E. Quarrington, and V. Roberts, *Phys. Rev.* **111**, 1245 (1958).
- D. E. Aspnes and A. A. Studna, *Phys. Rev. B* **27**, 985 (1983).
- S. E. Holland, D. E. Groom, N. P. Palaio, R. J. Stover, and M. Wei, *IEEE Trans. Electron Devices* **50**, 225 (2003).
- R. Hulthén, *Phys. Scr.* **12**, 342 (1975).
- R. A. Moffatt, N. A. Kurinsky, C. Stanford, J. Allen, P. L. Brink, B. Cabrera, M. Cherry, F. Insulla, F. Ponce, K. Sundqvist, S. Yellin, J. J. Yen, and B. A. Young, *Appl. Phys. Lett.* **114**, 032104 (2019); [arXiv:1807.07986 \[cond-mat.mtrl-sci\]](#).
- C. Stanford *et al.*, *AIP Adv.* **10**, 025316 (2020); [arXiv:1910.02169 \[cond-mat.mtrl-sci\]](#).
- B. Shank, D. Q. Nagasawa, J. J. Yen, M. Cherry, and B. A. Young, *J. Low Temp. Phys.* **167**, 202 (2012).
- B. Shank, D. Q. Nagasawa, B. Cabrera, M. Cherry, and B. A. Young, *J. Low Temp. Phys.* **176**, 148 (2014).
- Electrode was a tri-layer of 40 nm of W on 20 nm of Al on 40 nm of amorphous Si.
- K. Rajkanan, R. Singh, and J. Shewchun, *Solid-State Electron.* **22**, 793 (1979).
- V. P. Markevich, M. Vaqueiro-Contreras, J. T. De Guzman, J. Coutinho, P. Santos, I. F. Crowe, M. P. Halsall, I. Hawkins, S. B. Lastovskii, L. I. Murin, and A. R. Peaker, *Phys. Status Solidi A* **216**, 1900315 (2019).
- J. A. Hornbeck and J. R. Haynes, *Phys. Rev.* **97**, 311 (1955).
- Y. Hochberg, Y. Kahn, M. Lisanti, K. M. Zurek, A. G. Grushin, R. Ilan, S. M. Griffin, Z.-F. Liu, S. F. Weber, and J. B. Neaton, *Phys. Rev. D* **97**, 015004 (2018).
- S. M. Griffin, K. Inzani, T. Trickle, Z. Zhang, and K. M. Zurek, *Phys. Rev. D* **101**, 055004 (2020).
- N. Kurinsky, T. C. Yu, Y. Hochberg, and B. Cabrera, *Phys. Rev. D* **99**, 123005 (2019).
- S. M. Griffin, Y. Hochberg, K. Inzani, N. Kurinsky, T. Lin, and T. C. Yu, “SiC detectors for sub-GeV dark matter,” [arXiv:2008.08560 \[hep-ph\]](#) (2020).